



HAL
open science

Growth of monodisperse mesoscopic metal-oxide colloids under constant monomer supply

Koh Nozawa, Marie-Hélène Delville, Hideharu Ushiki, Pascal Panizza,
Jean-Pierre Delville

► **To cite this version:**

Koh Nozawa, Marie-Hélène Delville, Hideharu Ushiki, Pascal Panizza, Jean-Pierre Delville. Growth of monodisperse mesoscopic metal-oxide colloids under constant monomer supply. *Physical Review E: Statistical, Nonlinear, and Soft Matter Physics*, 2005, 72 (1), 011404 (8 p.). 10.1103/PhysRevE.72.011404 . hal-00015414

HAL Id: hal-00015414

<https://hal.science/hal-00015414>

Submitted on 15 May 2009

HAL is a multi-disciplinary open access archive for the deposit and dissemination of scientific research documents, whether they are published or not. The documents may come from teaching and research institutions in France or abroad, or from public or private research centers.

L'archive ouverte pluridisciplinaire **HAL**, est destinée au dépôt et à la diffusion de documents scientifiques de niveau recherche, publiés ou non, émanant des établissements d'enseignement et de recherche français ou étrangers, des laboratoires publics ou privés.

Growth of Monodisperse Mesoscopic Metal Oxide Colloids Under Constant Monomer Supply

Koh Nozawa^{§, #, †}, Marie-Hélène Delville^{#, a}, Hideharu Ushiki[†], Pascal Panizza[§], and

Jean-Pierre Delville^{§, b}

[§]Centre de Physique Moléculaire Optique et Hertzienne, UMR CNRS 5798, Université
Bordeaux I, 351 Cours de la Libération, 33405 Talence cedex, France

[#]Institut de Chimie de la Matière Condensée de Bordeaux, UPR CNRS 9048, Université
Bordeaux I, 87 Avenue du Dr. A. Schweitzer, 33608 Pessac cedex, France

[†]Laboratory of Molecular Dynamics and Complex Chemical Physics, Faculty of Agriculture,
Department of Environmental and Resource Science, Tokyo University of Agriculture and
Technology, 3-5-8, Saiwai-cho, Tokyo 183-8509, Japan

Abstract: In closed systems, control over the size of monodisperse metal oxide colloids is generally limited to submicrometric dimensions. To overcome this difficulty, we explore the formation and growth of silica particles under constant monomer supply. The monomer source is externally driven by the progressive addition into the system of one of the precursors. Monodisperse spherical particles are produced up to a mesoscopic size. We analyze their growth versus the monomer addition rate at different temperatures. Our results show that in the presence of a continuous monomer addition, growth is limited by diffusion over the investigated temporal window. Using the temperature variation of the growth rate, we prove that rescaling leads to a data reduction onto a single master curve. Contrary to the growth process, the final particles size reached after the end of the reagent supply, strongly

^a E-mail address: delville@icmcb-bordeaux.cnrs.fr

^b E-mail address: jp.delville@cpmoh.u-bordeaux1.fr

depends on the addition rate. The variation of the final particle size versus addition rate can be deduced from an analogy with crystal formation in jet precipitation. Within this framework, and using the temperature dependences of both the particle growth law and the final size, we determine the value of the molecular heat of dissolution associated to the silica solubility. These observations support the fact that classical theories of phase-ordering dynamics can be extended to the synthesis of inorganic particles. The emergence of a master behavior in the presence of continuous monomer addition also suggests the extension of these theories to open systems.

PACS Numbers: 81.07.-b, 81.20.Fw, 81.10.Dn, 82.60.Nh

I – INTRODUCTION

The synthesis of fine mesoscopic particles of targeted sizes is now required in numerous high technology applications as different as ceramics, catalysis, pigments, recording materials, medical diagnostics, or photonics^{1,2}. Since most physical properties of colloids are size dependent, it is essential to control their monodispersity as well as their uniformity in shape and composition. Reaching this goal requires a detailed understanding of both their mechanisms of formation and growth, under various experimental conditions. Classically, precipitation is initiated by fast quenching conditions, such as thermal quenching of a solution within the miscibility gap in which the solution becomes thermodynamically metastable³, or by pouring "instantaneously" a chemical species into another to initiate a chemical reaction⁴. These two situations are called conservative because their overall composition does not vary during the precipitation. For each case, the control over the synthesis of monodisperse particles up to mesoscopic scale is made difficult for two main reasons: (i) the segregation

intrinsically leads to polydispersity (due to the classical Lifshitz-Slyozov distribution ⁵, for instance) and, (ii) the monodispersity is limited to submicrometric dimensions for growth driven by chemical reactions ⁶. Even in seeded experiments ^{7, 8}, where growth is initiated using preformed nuclei, secondary nucleation cannot be avoided beyond a certain particle size (typically of the submicrometric order), preventing the formation of monodisperse mesoscopic particles. By contrast, experimental investigations of photographic colloid production by the double-jet technique ⁹ have shown that continuous changes in composition obtained by controlling the monomer source strongly improve particle monodispersity. The invoked reason is that particle growth proceeds in a starved situation as reagents are added ¹⁰. Moreover, as opposed to classical precipitation, the number of particles in solution asymptotically becomes constant and proportional to the addition rate when growth is limited by diffusion. This was experimentally and theoretically illustrated in the case of silver halides ^{11, 12}. However, despite these very appealing properties, such experimental procedures have been almost exclusively limited to the control of photographic colloids ^{11, 13}. With the exception of silver halides, to the best of our knowledge, the only experimental verification of the linear relation between particle number and addition rate concerns the synthesis of uniform *ZnO* particles. In a more general frame, such kinetic behaviors remain almost unexplored even if particle growth in open systems has recently received some confirmation in material-independent computer simulations at vanishing supersaturation ¹⁴. Confronting experimental results for different systems would certainly permit to check whether or not, nucleation and growth under continuous supply of monomer can be generalized to colloids other than silver halides. This is the purpose of our work, which is devoted to the formation of silica particles by inorganic polymerization.

We investigate the growth of monodisperse silica particles¹⁵ with diameter up to $2\ \mu\text{m}$ by controlling the effects of the progressive addition of an alcoholic solution of tetraethylorthosilicate (*TEOS*), defined herein as the monomeric precursor, in a hydro-alcoholic mixture of ammonia. This choice is motivated by the intrinsic importance of silica as one of the most familiar inorganic metal oxides, and by the common use of silica colloids in fundamental as well as practical research areas¹⁶.

The paper is organized as follows. In Sec. II, we describe the experimental procedures implemented to investigate the particle growth in open conditions. Sec. III is devoted to our experimental results whereas Sec. IV focuses on the theoretical background of particle growth for both closed and open configurations. In Sec. V, we then discuss our results. We finally conclude in Sec. VI with the opportunity offered by the present work to predict the properties of colloidal growth in open conditions.

II – SETUP AND EXPERIMENTAL CHARACTERIZATIONS

The preparation of monodisperse silica particles, first described by Kolbe¹⁷, generally proceeds with the hydrolysis and condensation of tetraalkoxysilanes (often tetraethylorthosilicate (*TEOS*) [$\text{Si}(\text{OR})_4$ with $R = \text{C}_2\text{H}_5$]) in a mixture of alcohol and water, with ammonia used as a catalyst^{18, 19}. Ultra pure water, *TEOS* ($\text{Si}(\text{OC}_2\text{H}_5)_4$, 99%, Aldrich Chemical Co.), ethanol ($\text{C}_2\text{H}_5\text{OH}$, J.T. Baker, 99.9%), and ammonia (NH_4OH , 28%, Aldrich Chemical Co.) are used as starting materials without further purification. The solutions are prepared at room temperature under inert argon atmosphere. The temperature of

the reactor is controlled with an accuracy of ± 0.05 °C by a thermoregulated bath (LAUDA, E200, ecoline SRE2312). The silica particles are grown by the hydrolysis of *TEOS* according to the following procedure . We first prepare separately two solutions I (5 ml *TEOS* in 30 ml ethanol) and II (9.5 ml aqueous ammonia in 50 ml ethanol). The total volume of solutions I and II, as well as the reagent concentrations, are the same for all our experiments. The overall molar ratio for *TEOS* / NH_3 / H_2O is 1/6.3/15.2 . This value is chosen in order to reach final particle diameters in the 1–2 μm mesoscopic range. Solution I is added at controlled flow rate by a syringe pump, under an argon blanket into the thermoregulated round bottom flask containing the solution II under mechanical stirring.

Analysis of the shape and the monodispersity of the produced SiO_2 particles is performed by transmission electron microscopy (JEOL JEM-2000 FX transmission electron microscope, using an accelerating voltage of 200 kV) at room temperature. Their growth is characterized by a homemade dynamic light scattering apparatus using a c.w. Ar^+ laser (wavelength in vacuum $\lambda_0 = 514$ nm) and an ALV5000 correlator. During the *TEOS* addition, we regularly pick one or two drops of solution in the reactor and quickly dilute them in 10 ml of alcohol in order to instantaneously stop the reaction. To increase the measurement accuracy, the mean particle size for each sample is then deduced by fitting the relaxation time of the correlation function versus the square modulus of the transfer wave vector for varying scattering angle θ .

III – EXPERIMENTAL RESULTS

III.1 – Effect of stirring speed on particle growth

To determine the relevant mechanisms involved in particle growth, we first check the influence of the stirring speed on the final particle size obtained well after the end of the *TEOS* addition. We perform a set of experiments for an addition rate of $125 \mu\text{l} / \text{min}$ at $T = 20 \text{ }^\circ\text{C}$ with stirring speeds varying between 300 and 700 rpm . For the whole set of attempts, we find a mean final particle radius $R_f = (480 \pm 10) \text{ nm}$. Such a good reproducibility is not surprising since the associated hydrodynamic Peclet number Pe , which compares the particle advection versus the solute diffusion within the reactor²⁰, is much smaller than unity. By definition, Pe is given by $Pe = \Omega R^2 / D_m$, where Ω , R and D_m are respectively the angular velocity associated to the stirring, the particle radius and the molecular diffusion coefficient of the monomer. Using the ethanol viscosity $\eta = 1.2 \times 10^{-3} \text{ Pa}\cdot\text{s}$ at $T = 20 \text{ }^\circ\text{C}$, as it constitutes more than 90% of the solvent phase at the end of the growth, and a typical monomer size $\sim 2 \text{ \AA}$, we find $D_m = 10^{-9} \text{ cm}^2/\text{s}$. On the other hand, the angular velocity Ω varies from 5 Hz (at 300 rpm) to 12 Hz (at 700 rpm). Since experiments lead to a final particle size $R_f \approx 500 \text{ nm}$, we find $10^{-3} \leq Pe \leq 3 \times 10^{-3}$ for the extreme values of the Peclet number. Consequently, the hydrodynamic effects at classical stirring velocities can totally be discarded for the investigation of particle growth. This is also illustrated by the particle growth laws presented below. Indeed, flow effects are known to significantly accelerate the kinetics compared to diffusion or reaction-limited growth²¹, a fact that is not observed in our experiments. In the following, we use an average stirring speed of 500 rpm .

III.2 –Particle growth law versus temperature and addition rate

We have undertaken a systematic study of the particle growth at different addition rates and for various temperatures. Measurements of the kinetic evolution of the particle size for three values of the addition rate Q ($Q = 68, 125, 250 \mu\text{l}/\text{min}$) performed at three different temperatures ($T = 0, 10, 20 \text{ }^\circ\text{C}$) are presented in Figure 1. These temperatures are chosen to fulfill the condition of negligible evaporation of the reagents in the argon atmosphere in order to keep their overall ratio constant in the solution. Mean particle radii were deduced from the following procedure. We measure for each sample the time τ_p associated to the exponential relaxation of the correlation function versus the scattering angle θ . Assuming that growing particles behave as Rayleigh scatterers, τ_p is given by $\tau_p = 1/2D_p q^2$, where

$D_p = k_B T / 6\pi\eta R$ is the mass diffusion of a particle of radius R , and $q = 4\pi n / \lambda_0 \sin(\theta/2)$ is the modulus of the transfer wave vector; n is the index of refraction of ethanol in which the few drops of solution are diluted. Then, by fitting the linear behavior of τ_p versus $1/q^2$, we obtain a reliable value of D_p and thus of R . An example of variation of $\tau_p (1/q^2)$ for various temporal samplings is given in Figure 2. The linear variation expected for Rayleigh particles is experimentally retrieved and we deduce the mean particle radius from the slope. The particle dynamics is also illustrated by TEM snapshots in Figure 3 for the "intermediate" couple ($Q = 125 \mu\text{l}/\text{min}$, $T = 10 \text{ }^\circ\text{C}$). The particle distribution appears to be highly monodisperse on the investigated temporal window, with an almost constant standard deviation smaller than 3%. This shows that the use of continuous addition of monomer offers the opportunity to easily push the limits of monodispersity up to the micrometer range while in closed systems it is always limited to the submicrometric sizes .

Figure 1 illustrates the dependence of the particle radius dynamics on the addition rate and the temperature. The growth can be divided in two parts: during and after the monomer supply.

During the monomer addition, two main features are observed: (i) the measured growth laws are very well separated in temperature and, (ii) the addition rate has no influence on them. As shown Figure 4, the variation of the particle radius versus time clearly exhibits a power law behavior with a mean measured exponent of $1/2$. By contrast, the final particle radius reached at the end of the monomer supply, strongly varies with the addition rate as well as the temperature.

IV – GROWTH IN OPEN SYSTEMS: THEORETICAL BACKGROUND

IV.1 – Particle growth rate

To interpret our data, let us extend the formulation of particle growth rate in closed systems to open ones. As particle growth does not depend on stirring, the concentration gradients do not couple with flow. The particle growth rate is, therefore, expected to be analogous to that found for unstirred constant composition systems²². It follows that growth is driven by the transportation of the monomers to the interface, here by diffusion, and then by their incorporation into the particle through interface interactions. If the monomer incorporation (respectively, the diffusion) is the fastest process, then growth is limited by diffusion (respectively, the interface kinetics). The growth rate dR/dt of a spherical particle of radius $R(t)$ is thus described by a general expression, which includes both bulk diffusion and interface reaction :

$$\frac{dR}{dt} = K_i \frac{(C(t) - C_{eq}(R))}{1 + \varepsilon R} . \quad (1)$$

$C(t)$ is the concentration of monomer at a given time t , and $C_{eq}(R)$ is the equilibrium concentration at the particle surface; in the following, concentrations are expressed as volume fractions. K_i is the rate constant for the surface integration of the monomer and ε^{-1} is a screening length which compares bulk diffusion to surface integration effect. ε is defined by $\varepsilon = K_i / (D_m \nu)$, where ν is the molecular volume of the precipitate. On the other hand, $C_{eq}(R)$ is classically given by the Gibbs-Thomson relation, yielding $C_{eq}(R) = C_s \exp(\alpha/R) \approx C_s (1 + \alpha/R)$, where C_s represents the bulk solubility, and $\alpha = 2\gamma\nu/k_B T$ is a capillary length. γ and k_B are respectively the liquid/particle surface energy and the Boltzmann constant. By defining the supersaturation σ as $\sigma(t) = (C(t) - C_s) / C_s$, the general expression of the particle growth rate becomes:

$$\frac{dR}{dt} = \frac{K_i C_s \alpha (1 - R_c/R)}{R_c (1 + \varepsilon R)}. \quad (2)$$

$R_c = \alpha/\sigma$ represents the critical radius above which a particle spontaneously grows and below which it dissolves. Eq. (2) shows that the transition from interface to diffusion limited growth is, indeed, controlled by the product εR . Growth is initially limited by the monomer incorporation at the particle surface ($\varepsilon R \ll 1$) and eventually becomes diffusion limited at large particle radius ($\varepsilon R \gg 1$). As we cannot estimate the value of ε (K_i being unknown), in the following, we briefly describe the particle growth laws expected in both cases.

As evidenced by Eq. (2), the particle growth strongly depends on the temporal behavior of the supersaturation σ . Usually, the kinetics of precipitation is divided in four main stages^{23, 24}.

(i) Due to the *TEOS* addition, the solute concentration initially increases linearly with time. At this stage, no particle nucleation exists. (ii) Spontaneous nucleation occurs as soon as the supersaturation reaches its critical value σ_c , i.e. when the activation energy for particle nucleation is of the order of $k_B T$. Particles are formed and grow. Due to the competition between growth and nucleation, σ reaches a maximum and then starts to decrease, and drops below σ_c . After this nucleation regime, (iii) a transient period appears where σ reaches a quasi-steady state corresponding to the so-called "free-growth regime". At this stage, σ becomes too low to allow the nucleation of new particles and the existing particles simply grow by drawing solute to their surface. (iv) Finally, due to the mass conservation, this free-growth regime cannot survive indefinitely, and therefore σ starts to decrease again towards its asymptotic value $\sigma = 0$. Consequently, the critical radius value significantly increases ($R_c \propto 1/\sigma$) and growth switches to the well-known Ostwald ripening regime, where the material resulting from the dissolution of some particles (those of radius $R < R_c$) is used by the others (those of radius $R > R_c$) to continue to grow. Note that, in the presence of monomer addition, there is a fifth additional regime. Indeed, when the dissolution of the smaller particles slows down, the surviving particles simply grow by the consumption of the incoming material that is continuously added to the system.

IV.2 – Free-growth regime

The particle growth in the free-growth regime is characterized by a constant supersaturation σ . Therefore, in the interface kinetic limited case ($\varepsilon R \ll 1$), Eq. (2) reduces to:

$$\frac{dR}{dt} = \frac{K_i C_s \alpha}{R_c} \left(1 - \frac{R_c}{R} \right). \quad (3)$$

Integration of Eq. (3) for $R/R_c \gg 1$ shows that the particle size increases linearly with time during the free-growth regime, i.e. $R \propto t$.

On the other hand, growth limited by diffusion presents different kinetic behaviors. In this case ($\varepsilon R \gg 1$), Eq. (2) becomes:

$$\frac{dR}{dt} = \frac{D_m \nu C_s \alpha}{R_c^2} \frac{(1 - R_c/R)}{R/R_c}. \quad (4)$$

For $R/R_c \gg 1$, integration of Eq. (4) reveals that the diffusion limited free-growth is characterized by a first $R \propto t$ behavior followed by an $R \propto t^{1/2}$ regime²⁵.

The particle number N remains constant during the free-growth regime²⁶, whatever the nature of the mechanism (interface kinetic or diffusion limited) governing the growth.

These growth mechanisms, which are analogous for both open and closed systems, have successfully been investigated in experiments involving liquid/liquid phase transitions. Their extension to inorganic colloid dispersions is much more recent. Dealing with closed systems,

an extensive study has shown that (i) silica beads grow by the incorporation of hydrolyzed monomers instead of aggregation of smaller particles and (ii) the late stage growth is limited by diffusion. A more recent investigation of the early stage growth of silica particles in closed conditions has revealed an $R \propto t$ regime followed by the behavior $R \propto t^{1/2}$. It has also been shown that the number of particles as well as their mass density remained nearly constant over the investigated reaction time period (from 50 to 2000 s). On the other hand, in an open system, Sugimoto has explored the growth of photographic emulsions versus addition rate at $T = 70^\circ\text{C}$. He showed that AgBr colloids grow as $R \propto t^{1/2}$, and that growth does not depend on the addition rate.

IV.3 – Ostwald ripening regime

As previously mentioned, σ cannot stay indefinitely constant due to the mass conservation, and therefore must decrease again. At this stage, growth switches from the free-growth regime to the well-known Ostwald ripening. The particles whose radius is smaller than the actual value of the critical radius, become unstable and dissolve, while larger ones continue to grow using the dissolved material. Nevertheless, due to the presence of monomer addition, the particle dissolution eventually stops. Consequently the surviving particles continue to grow mainly by consuming the flux of monomer that is continuously added to the system. As the nucleation rate is negligible during Ostwald ripening, the size distribution of particles

$f(R, t)$, defined by the particle number $N(t) = \int_0^\infty f(R, t) dR$, obeys a continuity equation:

$$\frac{\partial f}{\partial t}(R, t) + \frac{\partial}{\partial R} \left(\frac{dR}{dt} f(R, t) \right) = 0. \quad (5)$$

Since the supersaturation is vanishing, the conservation of the monomer concentration in the presence of addition, leads to:

$$\frac{4\pi}{3} \int_0^{\infty} f(R,t) R^3 dR = Qt . \quad (6)$$

Eqs. (3, 5, 6) show that the $R \propto t$ free-growth obtained for interface limited growth is followed by a ripening regime characterized by $R \propto t^{1/2}$ ²⁷, as for Ostwald ripening in closed systems . However, whereas for closed systems the particle number varies as $N \propto R^{-3}$ (i.e. $N \propto t^{-3/2}$), the matter conservation is different for open systems. One finds

$$N \propto \left[k_B T / (D_m C_s(T)) \right]^{3/2} Q/R, \text{ i.e. } N \propto t^{-1/2},$$

due to the source term associated to the monomer addition. On the other hand, for diffusion limited growth, Eqs. (4-6) show that the free-growth regime is followed by a ripening described by $R \propto t^{1/3}$; the same growth law is found for Ostwald ripening in closed systems²⁸. The variation of the number of particles also turns differently. In closed systems, the number of particles varies as $N \propto t^{-1}$ whereas it stabilizes to a stationary value $N \propto (k_B T Q) / (D_m C_s(T))$ for open systems¹⁴. This constant value also corresponds to the fixed number of particles found in the free-growth regime .

The confrontation of these predictions to published works on growth of inorganic colloids is not clear, even in closed systems. Indeed, very few experiments provide particle growth laws over significantly long time periods to lead to sufficiently reliable measured growth law exponent. In Pontoni's experiment on silica particles , a slow down in growth is observed

after the $R \propto t$ and $R \propto t^{1/2}$ measured regimes, but the transition towards the ripening regime is not clearly proved. This regime has nonetheless been recently observed in closed configuration by Oskam et al.²⁹ during the coarsening of different types of metal oxide nanoparticles (zinc and titanium oxide particles, for instance). On the other hand, we are not aware of any experiment on colloid growth dealing with Ostwald ripening in the presence of monomer addition.

V – DISCUSSION

V.1 – Particle growth rate in the presence of monomer addition

Coming back to our experiments, Figure 4 shows that the growth regime observed during the addition of *TEOS* corresponds to a $R \propto t^{1/2}$ behavior. The temporal exponents measured in Figure 4 are 0.65 ± 0.07 , 0.49 ± 0.02 , and 0.53 ± 0.03 , respectively, for $T = 0$, 10 , and 20 °C ; the apparently larger value obtained for $T = 0$ °C is explained in the following subsection. According to Sec. IV, the exponent $1/2$ found during the monomer addition can either corresponds to the generalized Ostwald ripening for interface limited growth or to the free-growth regime in the diffusion limited case. However, this exponent is obtained since the beginning of measurements, i.e. at a time where the supersaturation cannot be considered as negligibly small. Therefore, any possible link to Ostwald ripening is ruled out and the observed particle growth corresponds to the free-growth regime. This means that the particle growth had already switched from interface- ($\varepsilon R \ll l$) to diffusion-limited ($\varepsilon R \gg l$) at the beginning of the investigated temporal window. The diffusive origin of the measured growth law is also confirmed by the persistence of the $R \propto t^{1/2}$ regime just after the end of the

addition. Indeed, as soon as the addition is stopped, the system automatically switches from open to close. Accordingly, the particle growth law also switches to that corresponding for a closed configuration. Since the behavior $R \propto t^{1/2}$ is momentarily preserved, this means that growth is still limited by diffusion after the end of the addition. Finally, as in Pontoni's experiments, we do not identify the scaling regime $R \propto t^{1/3}$ associated to the Ostwald ripening between the free-growth regime and the saturation to the final particle size after the end of the *TEOS* addition.

V.2 –Rescaling of growth laws

We show that the particle growth law exponent illustrated in Figure 4 corresponds to the free-growth regime of diffusion limited growth, and that the associated amplitude only depends on temperature. Within the general framework of the kinetics of first-order phase transitions, a universal description of the particle growth should be retrieved for inorganic materials using Eq. (4). This is usually observed upon plotting the normalized particle radius $\rho = R/R_c$ versus the normalized time $\tau = D_m \nu C_s \alpha / R_c^3 t$ rescaled with the diffusive relaxation time scale associated to the critical radius R_c . However, for experiments which involve a continuous quenching³⁰ or addition of monomers, the initial supersaturation can no longer be defined. As a result, the value of the critical radius varies continuously, and then, prevents the use of the classical scaling considered for first-order phase transitions in closed systems. Nevertheless, the regular shift in temperature observed in Figure 1 supports the existence of some scaling in temperature. For the free-growth regime, where the supersaturation is constant, we find from Eq. (4):

$$R = \sqrt{(2D_m \nu C_s \sigma) t} . \quad (7)$$

A priori, three quantities vary with temperature: σ , D_m and C_s in Eq. (7). Since the behavior of σ is difficult to estimate for open systems, we assume that the supersaturation does not appreciably vary with temperature over the investigated range. On the other hand, one has

$$D_m \propto k_B T / \eta(T) \text{ where the shear viscosity is given by } \eta(T) = \eta_0 \exp(\Delta E_\eta / k_B T)^{31} \text{ and } \Delta E_\eta$$

is the shear stress activation energy. Finally, the silica solubility C_s depends on the molecular

heat of dissolution ΔE_s as $C_s \propto \exp(-\Delta E_s / k_B T)$. According to Eq. (7), this means that the

particle radius should rescale as $R \propto \sqrt{k_B T} \exp[-(\Delta E_\eta + \Delta E_s) / 2k_B T] \sqrt{t}$. The corresponding

fit for the temperature variation of the growth law amplitude is presented in the Inset of

Figure 4. We find $\Delta E = \Delta E_\eta + \Delta E_s = (0.5 \pm 0.1) \text{ eV}$ for the investigated temperature range.

Considering the temperature variation of the shear viscosity of the solution, here mainly

composed of ethanol³², we deduce $\Delta E_\eta = 0.14 \text{ eV}$. This leads to $\Delta E_s = (0.36 \pm 0.10) \text{ eV}$,

which is in very good agreement with already published data presented in Table 1. This value

is identical to that obtained by Hamrouni³³, and falls within the range of

$$\Delta E_s = (0.26 \pm 0.03) \text{ eV} \text{ to } \Delta E_s = 0.44 \text{ eV}^{34} \text{ found for the molecular heat of dissolution for}$$

silica. Then, according to Eq. (7), by plotting the particle growth laws presented in Figure 1

versus the rescaled time $\tau = (k_B T / \Delta E) \exp(-\Delta E / k_B T) t$, our data set should point out a single-

scaled dynamics for the growth during the monomer addition. This data reduction is shown in

Figure 5 for the whole set of experiments presented in Figure 1. The master curve also

enhances and demonstrates the existence of a well-defined crossover between the two regimes

$R \propto t$ and $R \propto t^{1/2}$ expected for diffusion limited free-growth. Indeed, even if the $R \propto t$

regime could be suspected in Figure 1 for the early growth observed at $T = 273 \text{ K}$, i.e. at low

temperature where the reaction rate is the slowest, it is now clearly identified by the scaling of the full data set. Note that the $R \propto t$ regime has already been observed in closed systems . Our data are nevertheless at variance with the late stage predictions for open systems as they do not even suggest the existence of an Ostwald ripening characterized by its $R \propto t^{1/3}$ behavior. Finally, the description of the particle growth by a master curve demonstrates a posteriori that the supersaturation does not appreciably vary with temperature during the monomer addition.

V.3 –Saturation of the particle growth

The observed scaling obviously breaks down, after some delay, when the addition of the monomer is stopped. Stopping the addition has two major consequences on the particle growth. From the fundamental point of view, the growth mechanisms change due to the switching from an open to a closed configuration. The $R \propto t^{1/2}$ is momentarily preserved, as illustrated in Figures 1 and 4 for time $t > t_Q$, and corresponds from now on to the free-growth regime in closed systems. Then, growth deviates towards a saturation of the particle radius. In contrast to particle growth performed in other metal oxide syntheses , Ostwald ripening for closed systems is not observed in our experiments. This is in good agreement with most of the experiments involving growth of silica particles, such as Pontoni's ones which do not show any Ostwald ripening either, when all the reagents are added together in a single step. This result could be explained by the experimental conditions required for silica particle synthesis, particularly in terms of pH of the solution, which are not strong enough to allow for silica dissolution . Then, the combination of both aspects, i.e. the formation of a set of monodisperse particles and the lack of observable Ostwald ripening, strongly suggests that the

constant number of particles N during the free-growth regime is preserved until the end of the growth, and thus corresponds to the final particle number. To check this assumption, we consider the available models of growth in open systems'. Based on particle growth limited by diffusion, they all show that the particle number N versus addition rate behaves as:

$$N = \beta \frac{Qk_B T}{8\pi D_m \gamma \nu C_S}, \quad (8)$$

where β is a numeric factor which depends on the chosen model ($1 \leq \beta \leq 3$); the most reliable theory gives $\beta = 1.57$. This prediction for free-growth limited by diffusion, particularly the behavior of N versus the addition rate Q , was experimentally verified in double-jet precipitation for silver halides production'' and also for inorganic metal oxide materials (zinc oxide colloid synthesis, for instance). Using mass conservation, the particle number N is related to the final radius R_f by:

$$N \frac{4}{3} \pi R_f^3 = v_{SiO_2}, \quad (9)$$

where v_{SiO_2} is the volume of produced silica corresponding to the added *TEOS*. By combining Eq. (8) and Eq. (9), the relation between the final particle radius and the addition rate becomes:

$$R_f = \left[\frac{6D_m \gamma v_{SiO_2} \nu C_S}{\beta k_B T} \right]^{1/3} Q^{-1/3}. \quad (10)$$

Consequently, in contrast to what occurs in the free-growth regime, the final particle size is expected to depend on the addition rate. The analogy with jet-precipitation leads to the behavior $R_f \propto Q^{-1/3}$. This predicted behavior, which is quantitatively demonstrated over more than two orders of magnitude in addition rate Q , is illustrated in Figure 6 for the experiments presented in Figure 1. Taking into account the investigated range of addition rates, the agreement is fairly good. Note that these measurements give an additional proof for diffusion limited growth since Ostwald ripening for interface limited growth in the presence and the absence of monomer addition are respectively characterized by $N \propto I/R \propto t^{-1/2}$ and $N \propto I/R^3 \propto t^{-3/2}$ (see Sec. IV.3), which cannot be supported by experimental data. Moreover, as predicted by Eq. (10) and observed in Figure 6, the final particle radius also varies with temperature. Using the temperature dependence of both the mass diffusion D_m and the silica solubility C_S , we should then be able to retrieve by an independent way, i.e. without considering the particle growth rate, the molecular heat of dissolution ΔE_S of silica. By forcing the exponent of the $R_f(Q)$ variation to be $-1/3$, we get the temperature behavior of the amplitude factor. It is expected to behave as $\exp(-\Delta E/3k_B T)$ from Eq. (10), where $\Delta E = \Delta E_\eta + \Delta E_S$. The corresponding fit is presented in the Inset of Figure 6. We find $\Delta E = \Delta E_\eta + \Delta E_S = (0.35 \pm 0.02) \text{ eV}$ for the investigated temperature range. Considering $\Delta E_\eta = 0.14 \text{ eV}$, this leads to $\Delta E_S = (0.21 \pm 0.02) \text{ eV}$. As illustrated in Table 1, this value is in good agreement with both the value previously deduced from particle growth laws and the few already published data^{16, 33, 34}.

VI – CONCLUSION

We have experimentally investigated the formation and the growth of monodisperse mesoscopic silica particles by analyzing the effects of the progressive addition of one of the reagents in the reactor. Our goal was twofold. At first, we wanted to implement a reliable technique to kinetically control colloid synthesis up to the microscopic size since classical methods usually fail for this length range (emergence of particle polydispersity). Indeed, the micron range is often considered as a sort of crossover between the nano- and the macro-world, called "mesoscopia"³⁵, that does not take advantage of the physical properties underlined by one or the other length scale. Then, we were interested in a description of metal oxide particle growth in terms of universal dynamic scaling, in order to discuss the existence of a unified picture within the classical first-order phase transition area.

To investigate the pertinence of the relevant external parameters, experiments were performed by varying the addition rate for different temperatures. In the presence of monomer addition, the formed silica particles are spherical and monodisperse all over the investigated size range (i.e. for particle radii R from 80 to 600 nm). At low Peclet number, measurements reveal that the growth of mesoscopic silica colloids is not affected at all by the monomer addition, but it simply depends on temperature. Moreover, the growth law exponents show that growth in the presence of continuous addition is limited by diffusion and corresponds to the so-called "free-growth regime", generalizing results already obtained in closed systems. As the temperature is the only relevant parameter during the monomer addition, the corresponding variation was used to rescale the dynamical data according to behaviors predicted for

diffusion limited growth. The data reduction onto a single master curve is clearly evidenced. This scaling also enhances the two particle growth laws expected for free-growth (i.e. $R \propto t$ and $R \propto t^{1/2}$) whereas the first one ($R \propto t$) is partly hidden in unscaled data. Finally, by using the temperature dependence of the amplitude of the particle growth, we have quantitatively deduced the molecular heat of dissolution of silica; the result compares very well with already published data. Consequently, our investigation strongly supports the fact that kinetic theories of first-order phase transitions can easily be applied to the growth of inorganic particles.

On the other hand, if the monomer addition is stopped, the observed master behavior cannot survive any longer. After some time delay, the particle growth irreversibly deviates from the scaled regime to asymptotically saturate to a final size. As opposed to the growth process, the final particle size is affected by the addition rate. Using an analogy with crystal formation in jet precipitation, we have explored the variations of the final particle size versus both the addition rate and the temperature. The power law expected theoretically for the variation of the final particle size versus addition rate is experimentally retrieved. A quantitative interpretation of the temperature behavior of the associated amplitude gives us the opportunity to determine, by a different way and independently from particle growth, the activation energy associated to the silica solubility.

More generally, our investigation may represent a first step toward a unified description of the processes involved in controlled colloid synthesis. Moreover, from a fundamental point of view, the observation of master behaviors for colloidal growth also brings new insights on the kinetic of precipitates in open systems^{36, 37}. Indeed, even for the most famous and spectacular example of coarsening in open system, the so-called “Liesegang phenomenon”³⁸ where the

precipitation of weakly soluble salts leads to periodic patterns, a close examination of the growth of the particles that form these patterns³⁹ still misses both theoretical developments and experimental investigations.

ACKNOWLEDGEMENTS

We thank T. Douar for technical assistance. This work was partly supported by the CNRS and the Conseil Régional d'Aquitaine.

TABLE CAPTION

Table 1: Molecular heat of dissolution of silica ΔE_s . Comparison between data published in the literature and the values obtained from the fits of both the measured particle growth laws and the addition rate dependence of the final particle sizes.

FIGURE CAPTIONS

Figure 1: Growth law of silica particles performed at temperatures $T = 0, 10, \text{ and } 20 \text{ }^\circ\text{C}$ for addition rates of TEOS $Q = 68, 125, \text{ and } 250 \text{ } \mu\text{l} / \text{min}$. A regime $R \propto t^{1/2}$ is evidenced during the monomer addition, while growth saturates to a final value R_f after the end of the addition. The arrows indicate the time t_Q corresponding to the end of the TEOS addition.

Figure 2: Linear variation of the relaxation time τ_p of the correlation function versus $1/q^2$ for particle solutions picked in the reactor at different times t during the growth and quickly diluted in ethanol. The slope increases with time since it is proportional to $1/D_p$ i.e. to $R(t)$. The experimental conditions correspond to $Q = 68 \mu\text{l}/\text{min}$ and $T = 20 \text{ }^\circ\text{C}$.

Figure 3: Transmission electron micrograph of silica particles showing their temporal behavior in terms of mean size \bar{R} , shape and monodispersity for $T = 10 \text{ }^\circ\text{C}$ and $Q = 125 \mu\text{l}/\text{min}$. (a) $t = 480 \text{ s}$, $\bar{R} = 101 \text{ nm}$; (b) $t = 1500 \text{ s}$, $\bar{R} = 195 \text{ nm}$, (c) $t = 2400 \text{ s}$, $\bar{R} = 265 \text{ nm}$, (d) $t = 3600 \text{ s}$, $\bar{R} = 335 \text{ nm}$; (e) $t = 7200 \text{ s}$, $\bar{R} = 420 \text{ nm}$. The bare scale is 200 nm .

Figure 4: Zoom on the particle free-growth regime $R(t) = \sqrt{\beta(T)t}$ expected from Eq. (7); symbols are the same as in Figure 1. Lines are power law fits with the forced growth exponent $1/2$ in order to deduce the amplitude $\beta(T)$. Note that experiments performed at the lowest temperature ($T = 10 \text{ }^\circ\text{C}$) present a larger growth exponent at the early stage (see text). The arrows indicate the time t_0 corresponding to the end of the TEOS addition. Inset: fit of the temperature variation of the amplitude $\beta(T)$ assuming a dependence in activation energy $\Delta E = \Delta E_\eta + \Delta E_s$, where ΔE_η and ΔE_s are respectively the activation energy associated to the shear viscosity of the solution and the molecular heat of silica dissolution.

Figure 5: Plot in rescaled time (R , $\tau = (k_B T / \Delta E) \exp(-\Delta E / k_B T) t$) of the nine experiments presented in Figure 1. The two successive regimes $R \propto \tau$ and $R \propto \tau^{1/2}$ expected for the diffusion limited particle free-growth are clearly evidenced by the data reduction onto a master curve.

Figure 6: Evolution of the final particle radius R_f versus the addition rate Q of TEOS for temperatures $T = 0, 10, \text{ and } 20 \text{ }^\circ\text{C}$. Lines are power law fits with the forced exponent $-1/3$ expected from Eq. (10). Inset: fit of the temperature variation of the associated amplitude assuming a dependence in activation energy $\Delta E = \Delta E_\eta + \Delta E_S$, where ΔE_η and ΔE_S are respectively the activation energy associated to the shear viscosity in the solution and the molecular heat of silica dissolution.

Table 1:

	R. K. Iler (Ref. [16])	B. Hamrouni <i>et al.</i> (Ref. [33])	R. A. Robie <i>et al.</i> (Ref. [34])	From particle growth: Eq. (7)	From final particle size: Eq. (10)
ΔE_s (eV)	0.26 ± 0.03	0.35	0.44	0.36 ± 0.10	0.21 ± 0.02

Figure 1:

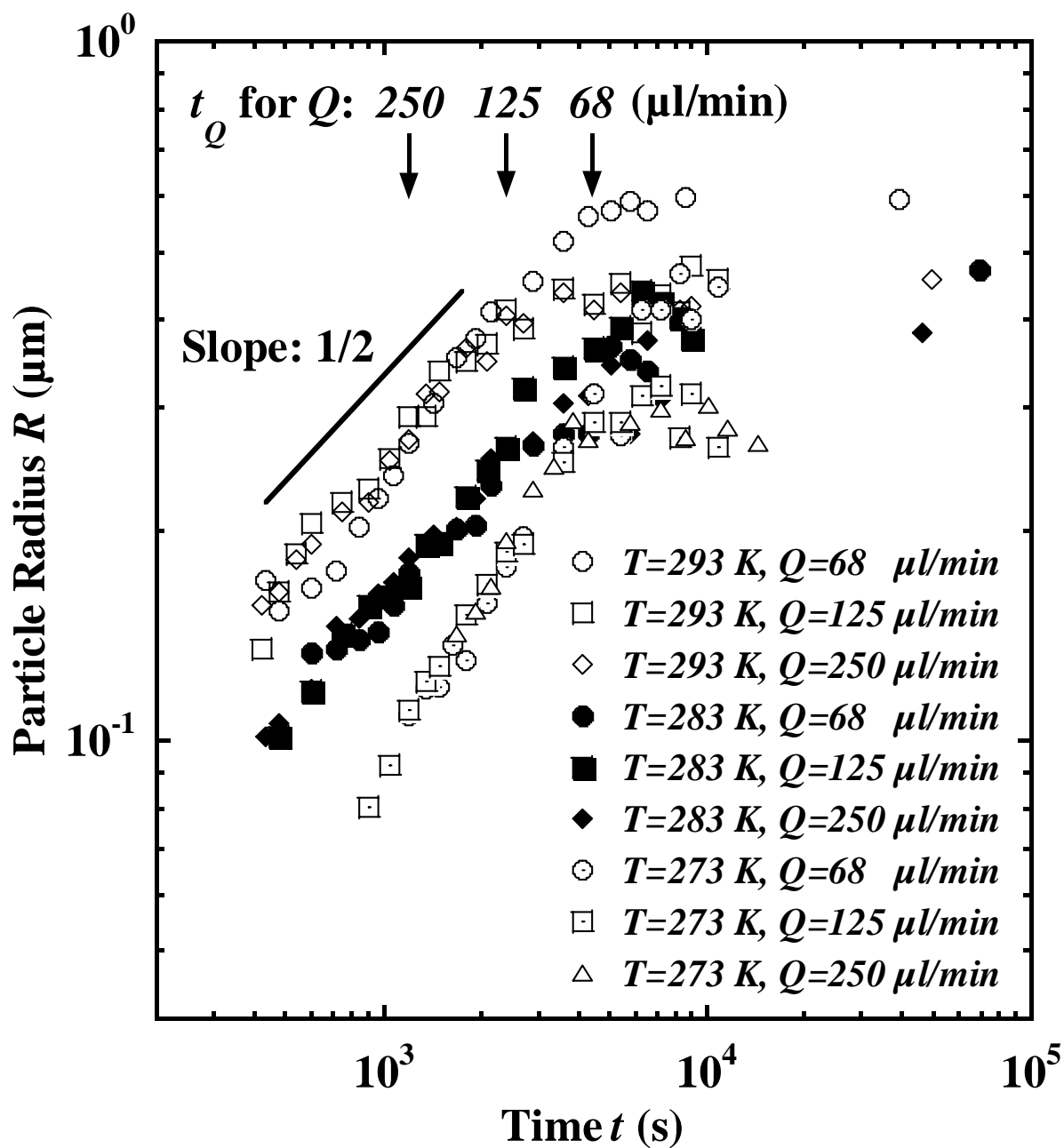


Figure 2:

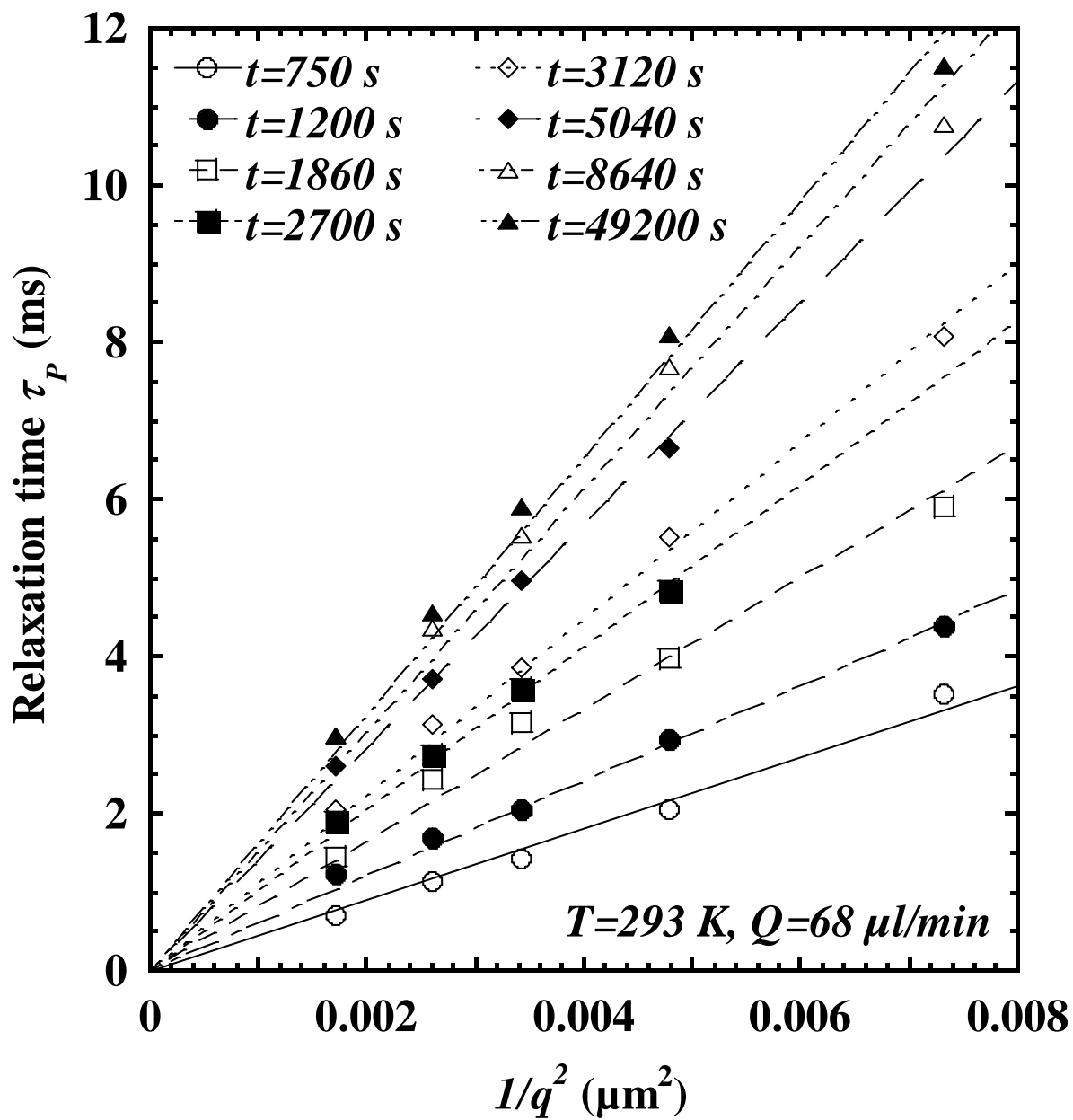


Figure 3:

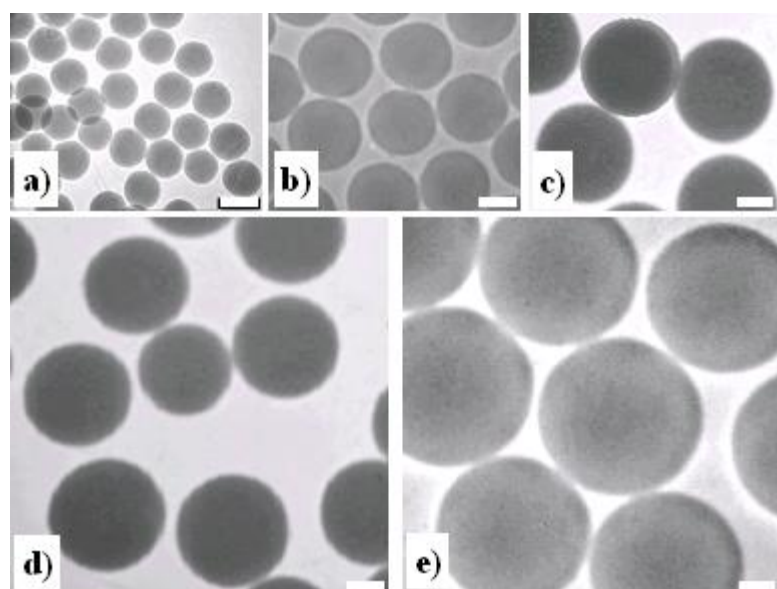


Figure 4:

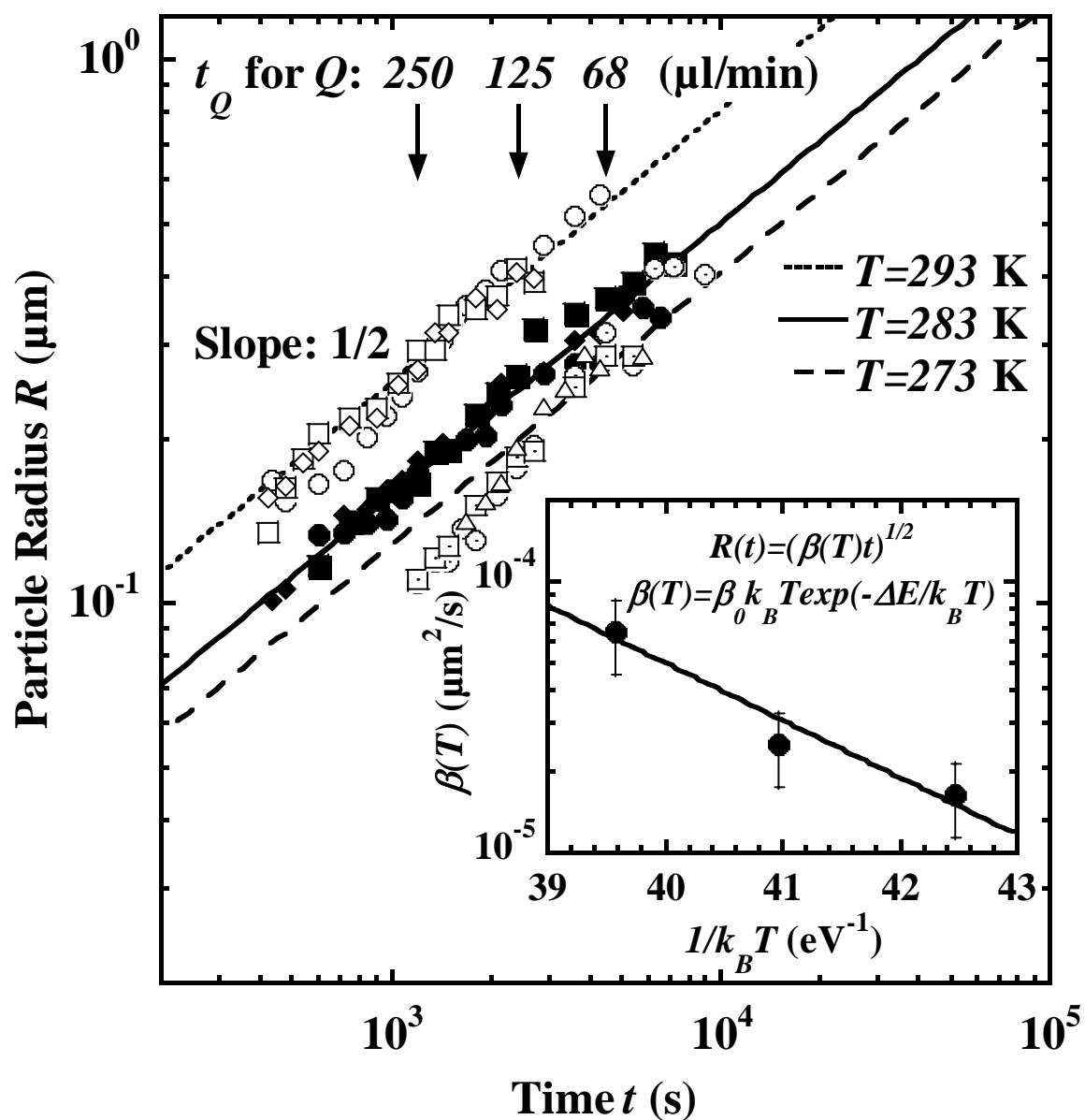


Figure 5:

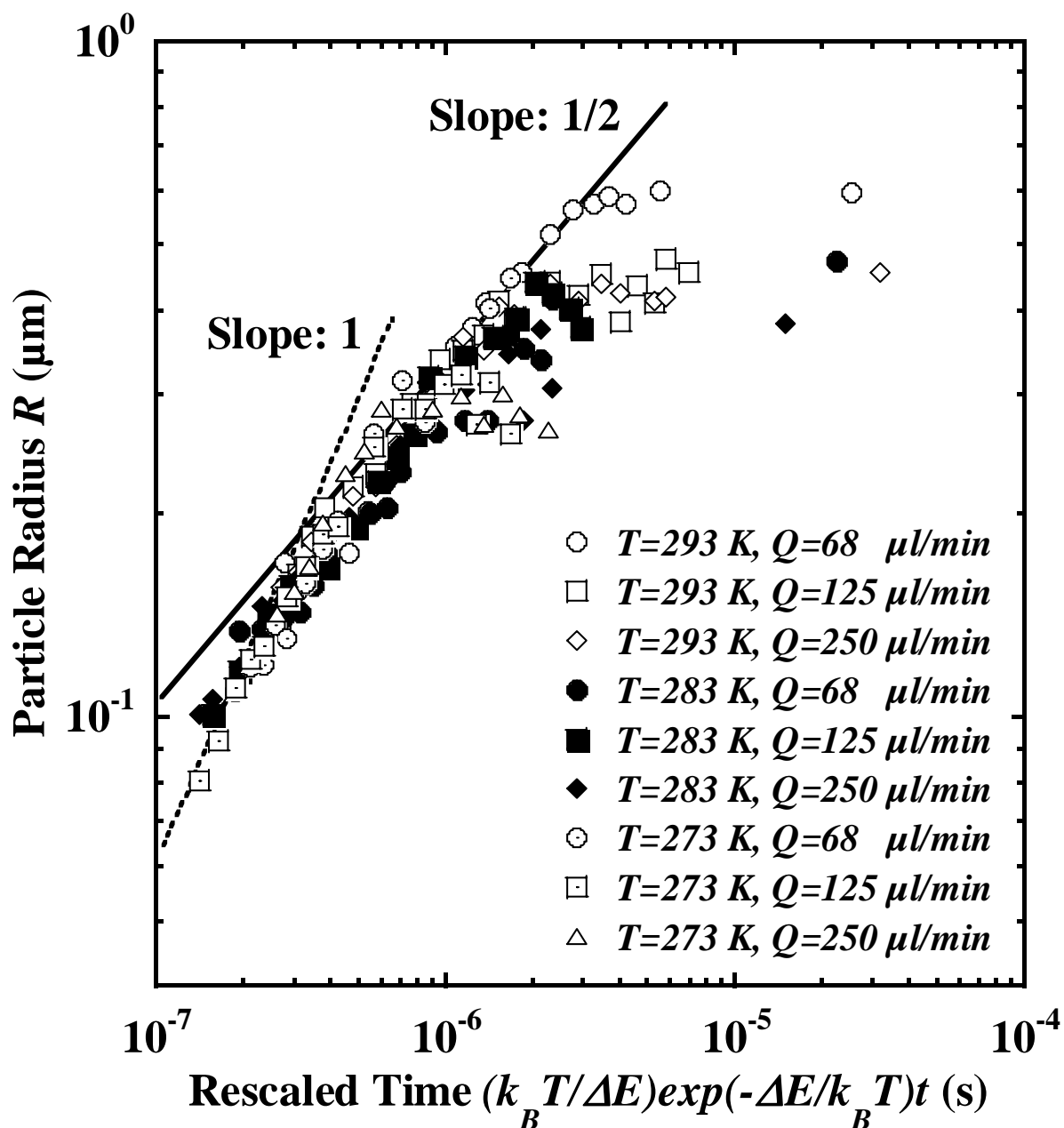
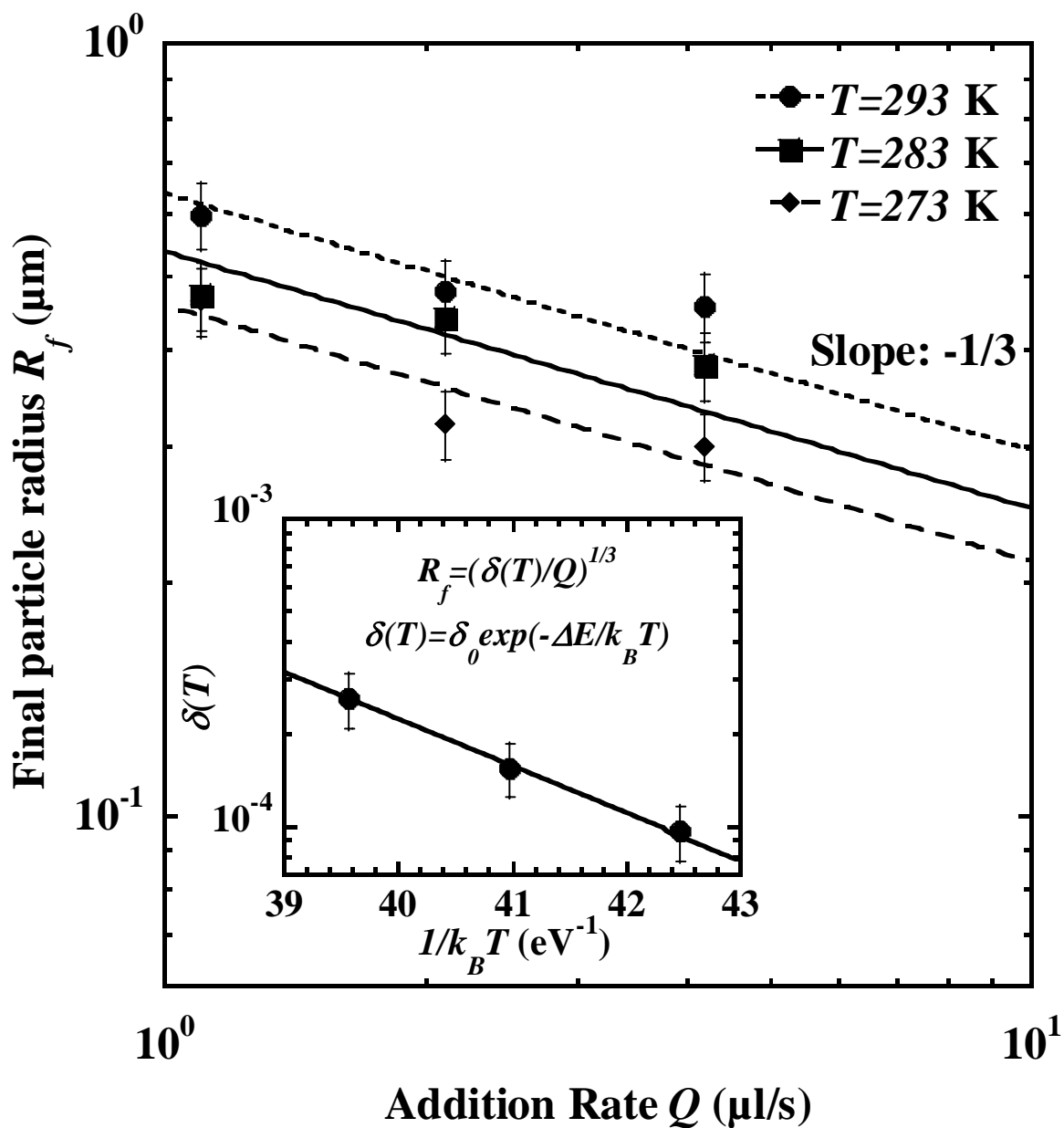


Figure 6:



REFERENCES

- ¹ M. I. Baraton, *Synthesis, Functionalization and Surface Treatment of Nanoparticles* (American Scientific Publishers, Stevenson Ranch, 2002).
- ² D. L. Feldheim and C. A. Foss, *Metal Nanoparticles: Synthesis, Characterization & Applications* (Marcel Dekker, 2001).
- ³ V. V. Slezov, J. Schmelzer, and Ya. Y. Tkach, *J. Chem. Phys.* **105**, 8340 (1996).
- ⁴ E. Matijević, *Langmuir* **10**, 8 (1994).
- ⁵ B. Meerson, *Phys. Rev. E* **60**, 3072 (1999).
- ⁶ G. H. Bogush, M. A. Tracy, and C. F. Zukoski, *J. Non-Cryst. Solids* **104**, 95 (1988).
- ⁷ S. L. Chen, P. Dong, G. H. Yang, and J. J. Yang, *J. Colloid Interface Sci.* **180**, 237 (1996).
- ⁸ K. Nozawa, H. Gailhanou, L. Raison, P. Panizza, H. Ushiki, E. Sellier, J.P. Delville, and M.H. Delville, accepted for publication in *Langmuir* (2005).
- ⁹ Q. Zhong and E. Matijević, *J. Mater. Chem.* **6**, 443 (1996).
- ¹⁰ S. K. Park, K. D. Kim, and H. K. Kim, *Colloids Surf. A: Physicochem. Eng. Aspects* **197**, 7 (2002).
- ¹¹ I. H. Leubner, *Current Opinion in Colloid & Interface Science* **5**, 151 (2000).
- ¹² T. Sugimoto, *J. Colloid Interface Sci.* **150**, 208 (1992).
- ¹³ I. H. Leubner, R. Jagannathan, and J. S. Wey, *Photogr. Sci. Eng.* **24**, 268 (1980); I. H. Leubner, *J. Phys. Chem.* **91**, 6069 (1987).
- ¹⁴ F. P. Ludwig and J. Schmelzer, *Z. Phys. Chem.* **192**, 155 (1995).
- ¹⁵ D. Pontoni, T. Narayanan, and A. R. Rennie, *Langmuir* **18**, 56 (2002).
- ¹⁶ R. K. Iler, *The Chemistry of Silica* (Wiley, New York, 1979).
- ¹⁷ G. Kolbe, *The Complex Chemical Behavior of Silica*, Dissertation, Jena, Germany 1956.
- ¹⁸ W. Stöber, A. Fink, and E. Bohn, *J. Colloid Interface Sci.* **26**, 62 (1968).

-
- ¹⁹ A. Van Blaaderen, V. J. Geest, and A. J. Vrij, *J. Colloid Interface Sci.* **154**, 481 (1992).
- ²⁰ T. Baumberger, F. Perrot, and D. Beysens, *Phys. Rev. A* **46**, 7636 (1992).
- ²¹ C. K. Chan and W. I. Goldberg, *Phys. Rev. Lett.* **58**, 674 (1987).
- ²² J. A. Marqusee and J. Ross, *J. Chem. Phys.* **79**, 373 (1983).
- ²³ A. J. Bray, *Adv. Phys.* **43**, 357 (1994).
- ²⁴ V. K. Lamer and R. H. Dinegar, *J. Am. Chem. Soc.* **72**, 4847 (1950).
- ²⁵ A. Cumming, P. Wiltzius, F. S. Bates, and J. H. Rosedale, *Phys. Rev. A* **45**, 885 (1992).
- ²⁶ M. Tokuyama and Y. Enomoto, *Phys. Rev. E* **47**, 1156 (1993).
- ²⁷ E. Brosh and A. Kiv, *J. Nucl. Mater.* **306**, 173 (2002).
- ²⁸ F. Perrot, P. Guenoun, T. Baumberger, D. Beysens, Y. Garrabos, and B. Le Neindre, *Phys. Rev. Lett.* **73**, 688 (1994).
- ²⁹ G. Oskam, Z. Hu, R. Lee Penn, N. Pesika, and P. C. Searson, *Phys. Rev. E* **66**, 011403 (2002).
- ³⁰ E. L. Huston, J. W. Cahn, and J. E. Hilliard, *Acta Metall.* **14**, 1053 (1966); S. Buil, J. P. Delville, and A. Ducasse, *Eur. Phys. J. E* **2**, 105 (2000).
- ³¹ E. Andrade, *Nature* **125**, 309 (1930).
- ³² *Handbook of Chemistry and Physics*, **52**th edition, edited by R. C. Weast (C. R. C., 1971)
- ³³ B. Hamrouni and M. Dhahbi, *Desalination* **136**, 225 (2001).
- ³⁴ R. A. Robie and D. R. Valdbaum, *US Geol. Survey Bull.* **1259**, 256 (1968).
- ³⁵ D. G. Grier, *Nature* **424**, 810 (2003).
- ³⁶ G. Venzl, *Phys. Rev. A* **31**, 3431 (1985).
- ³⁷ A. Nakahara, T. Kawakatsu, and K. Kawasaki, *J. Chem. Phys.* **99**, 9853 (1993).
- ³⁸ H. K. Henisch, *Periodic Precipitation* (Pergamon, 1991).
- ³⁹ M. E. LeVan and J. Ross, *J. Phys. Chem.* **91**, 6300 (1987).